The centriolar satellite proteins Cep72 and Cep290 interact and are required for recruitment of BBS proteins to the cilium

Timothy R. Stowe[a], Christopher J. Wilkinson[b], Anila Iqbal[b], and Tim Stearns[a,c]
[a]Department of Biology and [c]Department of Genetics, Stanford School of Medicine, Stanford, CA 94305-5020;
[b]Centre for Biomedical Sciences, School of Biological Sciences, Royal Holloway and Bedford New College, University of London, TW20 0EX Egham, United Kingdom

ABSTRACT **Defects in centrosome and cilium function are associated with phenotypically related syndromes called ciliopathies. Centriolar satellites are centrosome-associated structures, defined by the protein PCM1, that are implicated in centrosomal protein trafficking. We identify Cep72 as a PCM1-interacting protein required for recruitment of the ciliopathy-associated protein Cep290 to centriolar satellites. Loss of centriolar satellites by depletion of PCM1 causes relocalization of Cep72 and Cep290 from satellites to the centrosome, suggesting that their association with centriolar satellites normally restricts their centrosomal localization. We identify interactions between PCM1, Cep72, and Cep290 and find that disruption of centriolar satellites by overexpression of Cep72 results in specific aggregation of these proteins and the BBSome component BBS4. During ciliogenesis, BBS4 relocalizes from centriolar satellites to the primary cilium. This relocalization occurs normally in the absence of centriolar satellites (PCM1 depletion) but is impaired by depletion of Cep290 or Cep72, resulting in defective ciliary recruitment of the BBSome subunit BBS8. We propose that Cep290 and Cep72 in centriolar satellites regulate the ciliary localization of BBS4, which in turn affects assembly and recruitment of the BBSome. Finally, we show that loss of centriolar satellites in zebrafish leads to phenotypes consistent with cilium dysfunction and analogous to those observed in human ciliopathies.**

Monitoring Editor
Yixian Zheng
Carnegie Institution

Received: Mar 23, 2012
Revised: Jun 4, 2012
Accepted: Jun 29, 2012

INTRODUCTION

The animal cell centrosome functions in microtubule organization, cilium formation, cell division, polarity, and signaling. Centrosomes contain two centrioles that are duplicated once per cell cycle and are essential for the formation of cilia and flagella, evolutionarily conserved organelles that influence organismal development and homeostasis (Gerdes *et al.*, 2009). Ciliary assembly and recruitment of ciliary components are mediated by cooperation between intracellular trafficking and a process referred to as intraflagellar transport (IFT; Pedersen and Rosenbaum, 2008). Several signaling pathway receptors are localized to cilia and require this localization for the regulation of their respective pathways. In vertebrates, cilia are required for photoreceptor function, olfaction, and coordination of pathways such as Hedgehog, Wnt, and platelet-derived growth factor receptor-α (Pazour *et al.*, 2002; Huangfu *et al.*, 2003; Schneider *et al.*, 2005; Hunkapiller *et al.*, 2010).

In mammals, mutations in several genes encoding cilium and centrosome proteins have been identified that can lead to a shared set of phenotypes, including retinal degeneration, polydactyly, situs inversus, hydrocephaly, polycystic kidney disease, and neurocognitive defects. Diseases that result from defective centrosome/cilium function are collectively referred to as ciliopathies (Badano *et al.*, 2006; Baker and Beales, 2009) and include Joubert syndrome,

This article was published online ahead of print in MBoC in Press (http://www.molbiolcell.org/cgi/doi/10.1091/mbc.E12-02-0134) on July 5, 2012.

T.R.S. and T.S. designed, conducted, and analyzed experiments. T.R.S. and T.S. wrote the manuscript. C.J.W. designed and conducted zebrafish experiments with assistance from A.I.

Address correspondence to: Tim Stearns (stearns@stanford.edu).

Abbreviations used: BBS, Bardet–Biedl syndrome; GFP, green fluorescent protein; IFT, intraflagellar transport; MKS, Mekel–Gruber syndrome; OFD1, oral-facial-digital syndrome 1; PCM1, pericentriolar material 1.

nephronophthisis, Bardet–Biedl syndrome (BBS), oral-facial-digital syndrome 1 (OFD1), and Meckel-Gruber syndrome (MKS), all of which have a distinct but overlapping set of associated clinical features.

The molecular mechanisms underlying pathogenesis in the ciliopathies remain poorly understood (Hildebrandt *et al.*, 2011). For example, >100 unique mutations in the ciliopathy-associated gene *CEP290* have collectively been identified across several disorders (Coppieters *et al.*, 2010), including Joubert syndrome, MKS, and BBS (Valente *et al.*, 2006; Baala *et al.*, 2007; Brancati *et al.*, 2007; Leitch *et al.*, 2008). Depletion of Cep290 perturbs cilium formation and impairs ciliary recruitment of the ciliogenic small GTPase Rab8 (Kim *et al.*, 2008), yet the molecular function of Cep290 is not known. Experiments in the green alga *Chlamydomonas reinhardtii*, in which Cep290 localizes to the flagellar transition zone, implicate Cep290 in regulating the entry of proteins into the flagellum. *Chlamydomonas cep290* mutant flagella have abnormal levels of IFT proteins and the BBS-associated protein BBS4 (Craige *et al.*, 2010).

The proteins encoded by 7 of the 14 known BBS-associated genes assemble into a conserved ciliary-localized complex called the BBSome. The BBSome functions as a coat complex that traffics membrane proteins to cilia (Jin *et al.*, 2010) and can associate with Rabin8, the guanine nucleotide-exchange factor for Rab8 (Nachury *et al.*, 2007). BBS4-null mice are obese and exhibit retinal degeneration yet are able to form both motile and primary cilia (Mykytyn *et al.*, 2004). Interfering with BBS gene function in *Chlamydomonas* causes abnormal accumulation of signaling-related proteins in flagella (Lechtreck *et al.*, 2009). Together these observations suggest that BBS proteins function primarily by regulating transport of proteins associated with cilium function.

In mammals, both Cep290 and BBS4 localize to centriolar satellites (Kim *et al.*, 2004, 2008), 70- to 100-nm particles surrounding the centrosome. Centriolar satellites are defined by pericentriolar material 1 (PCM1), a large, 228-kDa coiled-coil protein originally identified as a centrosome-associated autoantigen (Balczon *et al.*, 1994; Kubo *et al.*, 1999), and are reported to function in dynein-dependent, microtubule-based trafficking of proteins to the centrosome (Dammermann and Merdes, 2002). Several proteins interact with PCM1 and localize to centriolar satellites, leading to the hypothesis that PCM1 functions as a scaffold for recruitment and delivery of these proteins (Kubo and Tsukita, 2003). Supporting this, depletion of PCM1 by RNA interference (RNAi) in mammalian cells results in loss of centriolar satellites and reduced centrosomal localization of some centriolar satellite-associated proteins (Dammermann and Merdes, 2002; Kim *et al.*, 2004, 2008; Kodani *et al.*, 2010). Centriolar satellites likely serve as a recruitment site for multiple ciliopathy-associated proteins, including BBS4, Cep290, and OFD1 (Lopes *et al.*, 2011). Whether this localization confers any functional regulation on these proteins remains unknown. Depletion of Cep290 results in the redistribution of centriolar satellites around centrosomes, possibly due to defective dissociation of centriolar satellites from dynein (Kim *et al.*, 2008). Of note, BBS4 is unique among PCM1-associated proteins in that ciliogenesis triggers the relocalization of BBS4 from centriolar satellites to primary cilia (Nachury *et al.*, 2007). However, the functional significance of BBS4 relocalization during cilium formation and the mechanisms that regulate it are unknown.

Here we address the broader role of centriolar satellites in centrosome and cilium function. We identify a new component of centriolar satellites, Cep72, a protein that had previously been implicated in mitotic spindle formation (Oshimori *et al.*, 2009), and discover a role for Cep72 and Cep290 in controlling the association of BBS4 with centriolar satellites through regulating its relocalization to the primary cilium. Finally, we show that PCM1 and centriolar satellites are important for cilium function in zebrafish.

RESULTS

Cep72 interacts with PCM1 and is a component of centriolar satellites

Cep72 was previously described as a centrosome protein (Andersen *et al.*, 2003; Oshimori *et al.*, 2009) and was found to interact with PCM1 in a high-throughput two-hybrid screen for interactions between human proteins (Rual *et al.*, 2005). Our analysis of human Cep72 revealed a related, uncharacterized protein, Lrrc36 (Figure 1). *CEP72* and *LRRC36* are part of a duplicated genome region in mammals; in humans, *CEP72* (Gene ID: 55722) is located at 5p15.33, and *LRRC36* (Gene ID: 55282) is at 16q22.1. In *Xenopus*, the genomic duplication is present, but one of the *CEP72/LRRC36* paralogues has been lost (Figure 1A). A single *CEP72/LRRC36* orthologue is present in chordates, deuterostomes, schistosomes, the cnidarian *Nematostella vectensis,* and the ciliated placozoan *Trichoplax adhaerens*, whereas no orthologue can be identified in *Chlamydomonas* or *Caenorhabditis elegans*. In organisms with a single *CEP72/LRRC36* gene, the predicted protein is more closely related to Cep72, suggesting that Cep72 represents the more ancient protein (Supplemental Figure S1A). Cep72 and Lrrc36 share a similar protein domain structure, consisting of conserved leucine-rich repeat (LRR) domains at the N-terminus and a coiled-coil domain at the C-terminus, flanking a central region lacking any identifiable domains (Figure 1B).

We examined the localization of Cep72 and Lrrc36 by coexpression of fusion proteins (Cep72-myc and Lrrc36–green fluorescent protein [GFP]) in cultured mammalian cells. Cep72-myc localized to foci resembling centriolar satellites, whereas Lrrc36-GFP was restricted to the centrosome (Supplemental Figure S1B). Deconvolution microscopy revealed extensive colocalization of Cep72-GFP with the centriolar satellite protein PCM1 (Figure 1C, top). In contrast, Lrrc36-GFP localized to the pericentriolar material of the centrosome, colocalizing with γ-tubulin (Figure 1C, bottom), and did not overlap with PCM1 (Supplemental Figure S1C). Thus, although Cep72 and Lrrc36 are related by gene duplication in mammals, localization to centriolar satellites is a unique property of Cep72.

We chose to study Cep72 in detail to further understand the function of centriolar satellites, first focusing on the association of Cep72 with PCM1 and centriolar satellites. An antibody directed against Cep72 (Supplemental Figure S1, D–I) recognized a protein of 72 kDa by Western blotting and also detected Cep72-GFP expressed in cells (Figure 1D). Immunofluorescence with this antibody showed that endogenous Cep72 localized to centriolar satellites in interphase cells, similar to tagged Cep72 expressed in stable transfectants (Figure 1E and Supplemental Figure S2A). Antibody reactivity and specificity were confirmed by blocking with GST-Cep72 antigen and by RNAi-mediated depletion of Cep72 (Supplemental Figure S1, D–I). Cep72 and PCM1 maintained their colocalization even when the normal distribution of centriolar satellites was disrupted by treatment with nocodazole or expression of p50 dynamitin (Supplemental Figure S2, B and C).

Given the colocalization of Cep72 and PCM1, we tested whether the two proteins interact in vivo. Immunoprecipitation of endogenous PCM1 from hTERT-RPE1 cells coprecipitated endogenous Cep72 (Figure 1F). This interaction was confirmed by coimmunoprecipitation of ^{LAP}Cep72 and endogenous PCM1 from ^{LAP}Cep72-IMCD3 cells (Figure 1G). Together these results suggest that Cep72 localizes to centriolar satellites by virtue of an interaction with PCM1. Also, the pattern of evolutionary conservation for Cep72 is similar to

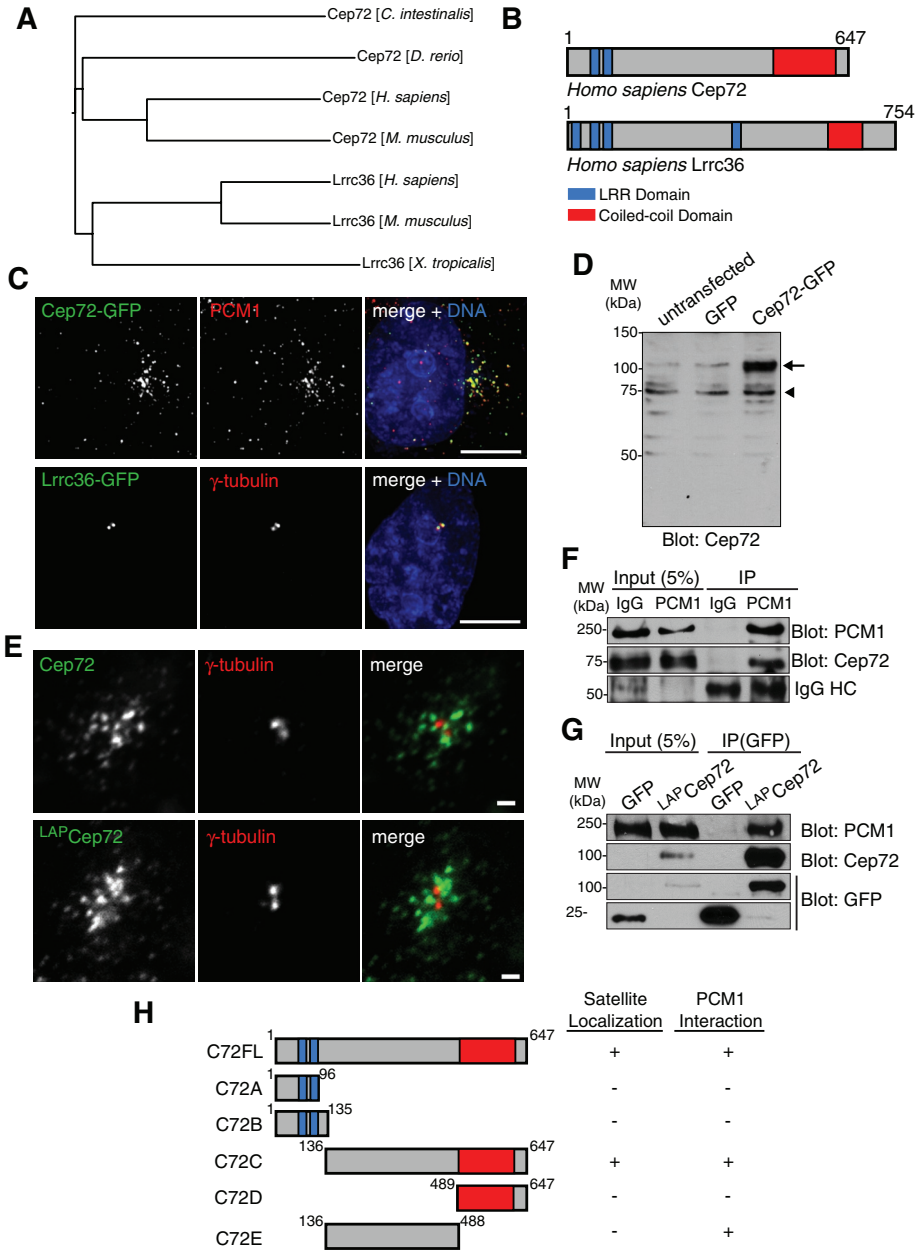

FIGURE 1: Cep72 is a component of centriolar satellites and interacts with PCM1. (A) Phylogenetic dendrogram showing the relationship between a subset of *CEP72* and *LRRC36* orthologues. Multisequence alignments were computed with Tcoffee. (B) Protein domain schematic for Cep72 and Lrrc36. Both proteins contain leucine-rich repeat (LRR) domains (blue) and a coiled-coil domain (red), as indicated. (C) Cep72 localizes to centriolar satellites, and Lrrc36 localizes to the pericentriolar material of the centrosome. hTERT-RPE1 cells were transfected with GFP-tagged Cep72 or Lrrc36 expression constructs, fixed, and immunostained for Cep72-GFP (anti-GFP) and PCM1 (top) or Lrrc36-GFP (anti-GFP) and γ-tubulin (bottom). DNA was stained with 4′,6-diamidino-2-phenylindole (DAPI). Scale bars, 5 μm. (D) Extracts from control, GFP, or Cep72-GFP transfected 293 cells were probed with Cep72 antibody. Cep72-GFP (arrow) and endogenous Cep72 (arrowhead) are indicated. (E) Localization of Cep72 in interphase. HeLa cells were fixed and immunostained for endogenous Cep72 and γ-tubulin (top). Stably expressing ^{LAP}Cep72-IMCD3 cells were stained for ^{LAP}Cep72 (anti-GFP) and γ-tubulin (bottom). DNA was stained with DAPI. Scale bars, 1 μm. (F) Endogenous PCM1 was immunoprecipitated from hTERT-RPE1 cell extracts using anti-PCM1 or rabbit IgG as a control. Immunoprecipitates were probed for endogenous PCM1 and Cep72. (G) Immunoprecipitation of GFP or ^{LAP}Cep72 was performed on extracts from GFP-expressing IMCD3 cells or ^{LAP}Cep72-IMCD3 cells using a GFP antibody. Immunoprecipitates were probed for GFP, ^{LAP}Cep72 (anti-GFP or anti-Cep72), and endogenous PCM1. (H) Schematic of Cep72 deletion constructs and summary of their localization and interaction with PCM1. Colocalization was determined by analyzing NIH 3T3 cells transfected with GFP-tagged deletion constructs and immunostaining fixed cells with anti-GFP and anti-PCM1. Interaction was determined by coimmunoprecipitation of GFP-tagged deletion constructs and PCM1 from extracts of transfected NIH 3T3 cells. Both C72FL (full-length) and C72C were able to interact with PCM1 and localize to satellites, as determined by observation of a normal, pericentrosomal distribution of GFP-positive puncta that colocalized with PCM1. C72E interacted and colocalized with PCM1 but formed cytoplasmic aggregates with a distribution that differed from that of normal satellites.

that for PCM1 (Hodges *et al.*, 2010), consistent with the interaction that we observed.

Cep72-deletion constructs were used to determine the domains required for interaction with PCM1 and localization to centriolar satellites (Figure 1H and Supplemental Figure S3). A fragment of Cep72 lacking the first 136 amino acid residues (C72C) was sufficient for localization to centriolar satellites and interaction with PCM1. The central region of Cep72, lacking both the coiled-coil domain and LRR domains (C72E) was able to interact with PCM1 but disrupted centriolar satellites by forming large aggregates that sequestered PCM1. These data suggest that interaction of Cep72 with PCM1 is required for localization of Cep72 to centriolar satellites and that the central region of Cep72 likely mediates this interaction.

Effects of PCM1 depletion on localization of centriolar satellite proteins

We used depletion of PCM1 to determine the effects of loss of centriolar satellites (Kubo *et al.*, 1999; Ge *et al.*, 2010) on the localization of Cep72 and two other components of centriolar satellites—BBS4 and Cep290—based on their importance in ciliopathies. Expression of an shRNA targeting PCM1 efficiently depleted the protein, as assessed by Western blot and immunofluorescence (Figure 2A and Supplemental Figure S4A).

We considered BBS4 first, following on the initial characterization by Nachury *et al.* (2007). As described previously (Nachury *et al.*, 2007), PCM1 depletion in nonciliated cells resulted in loss of centriolar satellites and dispersion of BBS4 throughout the cytoplasm (Supplemental Figure S4B). Nachury *et al.* (2007) showed that the total level of BBS4 is not altered in PCM1-depleted cells, and thus the apparent reduction in immunofluorescence signal is presumably due to the absence of focused localization. In cells with a primary cilium,

BBS4 relocalizes from centriolar satellites to the primary cilium (Figure 2B; Nachury *et al.*, 2007), whereas other satellite proteins, including Cep72, are retained in satellites (Supplemental Figure S4C). Although PCM1 depletion reduced the efficiency of ciliogenesis in hTERT-RPE1 cells (Figure 2C) as previously reported (Nachury *et al.*, 2007; Kim *et al.*, 2008), some PCM1-depleted cells did form cilia, and in these cells, localization of BBS4 to the cilium occurred normally, in the absence of centriolar satellites (Figure 2D). Therefore PCM1 and centriolar satellites are dispensable for ciliary localization of BBS4.

Loss of PCM1 resulted in a striking relocalization of ^{LAP}Cep72 from centriolar satellites to the centrosome in both ciliated and nonciliated cells (Figure 2E and Supplemental Figure S5, A and B). A similar relocalization to the centrosome was observed for endogenous Cep72 in PCM1-depleted HeLa cells (Figure 2F). This change reflects new localization of Cep72 to the centrosome rather than retention of a minor pool of centrosome-localized Cep72 that might have been obscured by the brighter satellites, as deconvolution microscopy showed that neither Cep72 nor PCM1 localized to the centrosome in cells in which the centrosome was visibly separate from satellites (Supplemental Figure S5C). In addition, the centrosomal relocalization of Cep72 in PCM1-depleted cells was not dependent on microtubules (Supplemental Figure S5D) and persisted in mitotic cells (Supplemental Figure S5E).

Kim *et al*. (2008) examined the localization of Cep290 in PCM1-depleted cells and reported loss of centriolar satellite–localized Cep290 and retention of centrosome-localized Cep290. As for Cep72, we tested whether the altered Cep290 localization in PCM1-depleted cells might instead reflect a relocalization of Cep290. In control cells, Cep290 localized to centriolar satellites (Chang *et al.*, 2006; Kim *et al.*, 2008), as well as to larger structures adjacent to, but distinct from, the centrosome, as defined by γ-tubulin staining (Figure 2G, top, and Supplemental Figure S6A). In PCM1-depleted cells, Cep290 was absent from centriolar satellites and colocalized with centrosomal γ-tubulin (Figure 2, bottom). These results suggest that the association of Cep72 and Cep290 with centriolar satellites restricts them from localizing to the centrosome.

Cep72 is required for recruitment of Cep290 to centriolar satellites and normal distribution of centriolar satellites

Cep72 and Cep290 localize to satellites and respond similarly to depletion of PCM1. Therefore we examined the relationship between them. By immunofluorescence, Cep72 and Cep290 partially colocalized in centriolar satellites (Supplemental Figure S6A), and immunoprecipitation of Cep72-GFP coprecipitated endogenous Cep290, as well as PCM1 (Figure 3A). We next tested whether Cep72 and Cep290 depend on one another for localization to centriolar satellites. Effective depletion of Cep72 and Cep290 was verified by Western blot and immunofluorescence of siRNA-transfected cells (Figure 3, B and C). Cep72 localized normally to satellites in cells depleted of Cep290 (Supplemental Figure S6B). In contrast, there was a significant ($p < 0.001$) reduction in the amount of centriolar satellite–associated Cep290 in cells depleted of Cep72 (Figure 3, D and E). Altered localization of Cep290 was likely a direct consequence of the loss of Cep72, as Cep72 depletion neither reduced Cep290 protein level (Supplemental Figure S6C) nor had any observable effect on organization of the interphase microtubule cytoskeleton (Supplemental Figure S6D and previously reported; Oshimori *et al.*, 2009).

Depletion of Cep290 has been reported to result in redistribution of centriolar satellites, increasing their concentration around the centrosome (Kim *et al.*, 2008). Because Cep72 was required for localization of Cep290 to centriolar satellites, we tested whether depletion of Cep72 resulted in a similar redistribution of centriolar satellites, as determined by PCM1 localization. Individual depletion of either Cep72 or Cep290 resulted in both a significant ($p < 0.001$) increase in the amount of pericentrosomal PCM1 and a corresponding reduction in cytoplasmic centriolar satellites, as determined by quantitative immunofluorescence (Figure 3, F and G, and Supplemental Movies S1 and S2). This redistribution of centriolar satellites was dependent on an intact microtubule cytoskeleton and likely reflects a clustering of satellites around the centrosome (unpublished data).

We next tested whether Cep72, like Cep290 (Nachury *et al.*, 2007; Kim *et al.*, 2008; Tsang *et al.*, 2008), is required for efficient ciliogenesis in hTERT-RPE1 cells. Depletion of Cep290 significantly ($p < 0.001$) reduced cilium formation in serum-starved cells, whereas Cep72 depletion caused a more modest but significant ($p < 0.05$) reduction (Figure 3H and Supplemental Figure S6E). To test whether the Cep72-related paralogue Lrrc36 might be partially compensating for Cep72 loss in this context, we tested whether concurrent depletion of Cep72 and Lrrc36 would exacerbate the observed ciliogenesis phenotype. Depletion of Lrrc36 did not affect ciliogenesis, and codepletion of Lrrc36 and Cep72 resulted in a phenotype similar to depletion of Cep72 alone (Supplemental Figure S7, A and B).

Overexpression of Cep72 disrupts organization of centriolar satellites and interferes with primary cilium formation

Overexpression of Cep290 or BBS4 disrupts centriolar satellite distribution and results in the formation of aggregates that sequester PCM1 (Kim *et al.*, 2004, 2008; Vladar and Stearns, 2007). We tested the effects of Cep72 overexpression on centriolar satellites. In low-expressing cells, Cep72-GFP colocalized with PCM1 to centriolar satellites, similar to endogenous Cep72. However, in high-expressing cells, Cep72-GFP formed cytoplasmic aggregates (Figure 4A) that sequestered endogenous PCM1, with a corresponding reduction in pericentrosomally distributed centriolar satellites (Figure 4A, inset). In some cells, these aggregates also sequestered BBS4-myc and Cep290 (Figure 4B). This sequestration phenotype was specific to centriolar satellite proteins, as Cep72 overexpression did not affect the localization of other centrosomal proteins (γ-tubulin and centrin, Figure 4B; pericentrin, ninein, and dynein, Supplemental Figure S7C). We also observed sequestration of Rab8-GFP in Cep72 aggregates in some cells, consistent with the reported interaction of Cep290 and Rab8 (Supplemental Figure S7C; Nachury *et al.*, 2007; Kim *et al.*, 2008; Tsang *et al.*, 2008). Cep72-GFP aggregates that formed in cells depleted of PCM1 were still able to sequester Cep290 but not BBS4, suggesting that Cep72 and Cep290 can interact in the absence of PCM1 (Figure 4D). In serum-starved hTERT-RPE1 cells, overexpression of Cep72 resulted in a significant ($p < 0.05$) decrease in the fraction of ciliated cells (22 ± 7.8%, $n = 300$) as compared with control cells (78 ± 4.3%, $n = 300$) or GFP-expressing cells (66 ± 4.6%, $n = 300$; Figure 4C).

Cep72 and Cep290 are required for relocalization of BBS4 from centriolar satellites to primary cilia during ciliogenesis

Because centriolar satellites are not required for the recruitment of BBS4 to the cilium, we tested whether the association of BBS4 with satellites might instead regulate that recruitment. In *Chlamydomonas*, which lacks an identifiable PCM1 orthologue. Cep290 is localized to the flagellar transition zone and functions in regulating flagellar protein content (Craige *et al.*, 2010). Given the unique localization of mammalian Cep290 to both the transition zone (Garcia-Gonzalo *et al.*, 2011) and centriolar satellites, we reasoned that Cep290 might exert some part of its regulatory function at satellites in mammalian

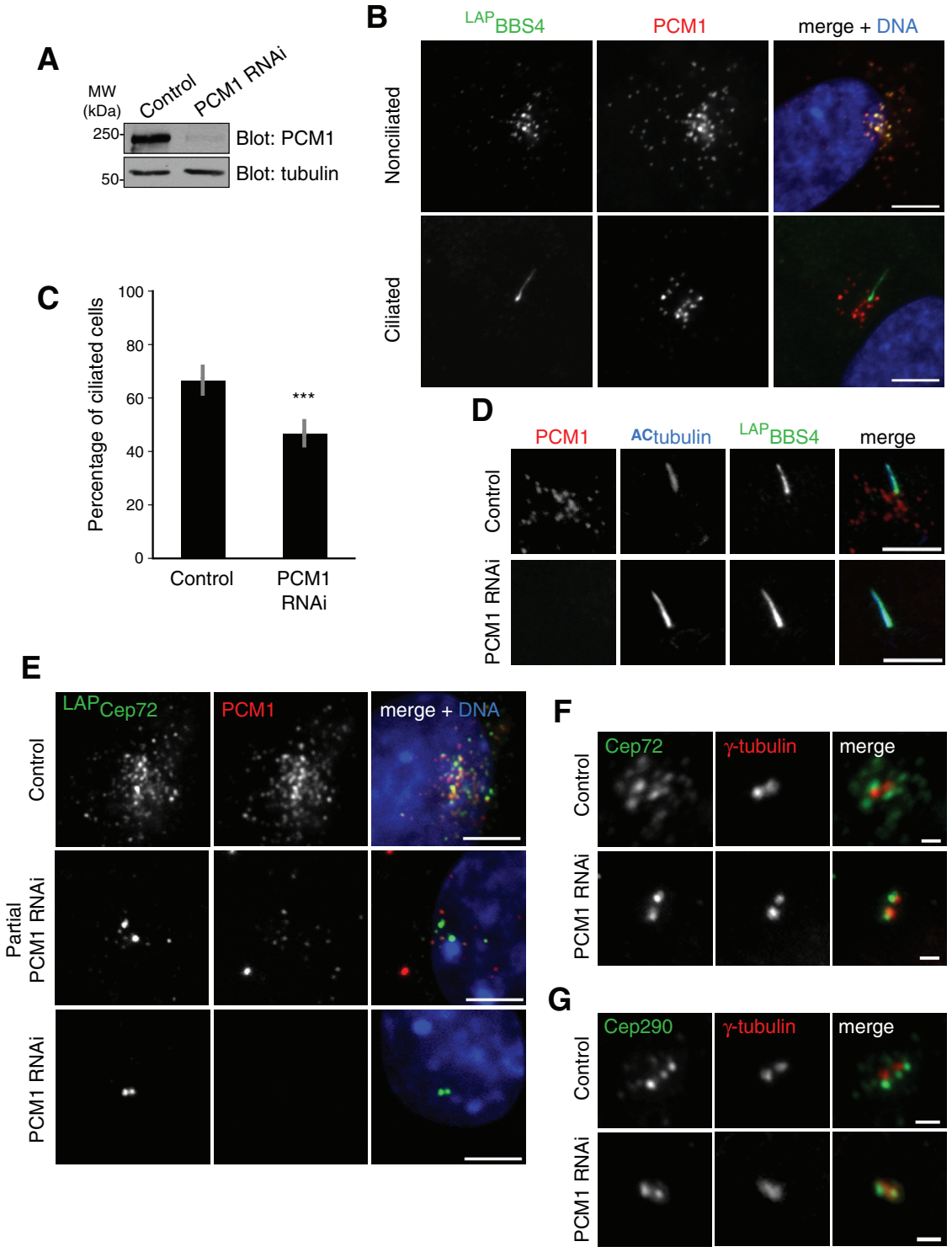

FIGURE 2: Effects of PCM1 depletion on localization of centriolar satellite proteins. (A) Western blot analysis of extracts from control or PCM1 RNAi IMCD3 cells, selected for transfection with control or PCM1 shRNA-expressing plasmids, probed with anti-PCM1 or anti–α-tubulin, as a loading control. (B) ^{LAP}BBS4-hTERT-RPE1 in asynchronous (top) or serum-starved (bottom) populations were fixed and immunostained for ^{LAP}BBS4 (anti-GFP) and endogenous PCM1. After serum starvation, BBS4 is absent from centriolar satellites and localizes to the primary cilium. DNA was stained with DAPI. Scale bars, 5 μm. (C) Control and PCM1-depleted hTERT-RPE1 cells were serum starved for 24 h, fixed, and immunostained for acetylated tubulin to label primary cilia. Percentage of ciliated cells was determined in each case. Control, $n = 700$; PCM1 depleted, $n = 500$. Error bars, SEM. ***$p < 0.001$, *$p < 0.05$. (D) Centriolar satellites are not required for ciliary recruitment of BBS4. Localization of ^{LAP}BBS4 (anti-GFP) and PCM1 in ciliated control (top) and PCM1-depleted (bottom) ^{LAP}BBS4-hTERT-RPE1 cells. Cilia are labeled with anti–acetylated tubulin (^{AC}tubulin). Scale bars, 5 μm. Note that in the absence of PCM1 (loss of centriolar satellites), ^{LAP}BBS4 still localizes to primary cilia. (E) PCM1 depletion results in relocalization of Cep72 to the centrosome. ^{LAP}Cep72-IMCD3 cells were transfected with control or

cells. To test this, we assessed the localization of BBS4 in ciliated cells depleted of Cep72 or Cep290. As for PCM1 depletion, ciliogenesis was decreased in Cep290- and Cep72-depleted cells (Figure 3H), but some cells did form a cilium and were assayed here. A significant ($p < 0.005$) reduction in the fraction of cilia containing ^{LAP}BBS4 relative to control ciliated cells (72 ± 3.5% of total) was observed for cells depleted of Cep72 (39 ± 4.9% of total) or Cep290 (33 ± 4.5% of total). In many such cells, ^{LAP}BBS4 remained associated with centriolar satellites rather than localizing to the cilium (Figure 5, A and C), a distribution that was not observed in control cells.

BBS4 is the only BBSome subunit that localizes to centriolar satellites, and it is the final subunit added during assembly of functional BBSome complex (Zhang *et al.*, 2012). We tested whether failure of BBS4 to properly localize to cilia in cells depleted of Cep290 or Cep72 cells might also result in a defect in ciliary localization of the BBSome. Localization of the BBSome subunit BBS8 was assessed in cells depleted of Cep72 or Cep290. In control cells, BBS8 localized to the base of the primary cilium or throughout the length of the cilium, as assessed by colocalization with acetylated α-tubulin (44 ± 5.9% of total). However, there was a significant ($p < 0.001$) decrease in the fraction of BBS8-positive cilia in cells depleted of Cep72 (3.1 ± 1.9% of total) or Cep290 (10 ± 1.7% of total) as compared with control (Figure 5, B and D). Thus disruption of centriolar satellite function by depletion of Cep72 or Cep290, as opposed to loss of satellites by depletion of PCM1, results in a failure of BBS4, BBS8, and presumably the BBSome as a whole to localize to the cilium; this suggests that centriolar satellites might regulate recruitment of BBS proteins to the cilium through sequestration and release of BBS4 during ciliogenesis.

Loss of centriolar satellites causes cilium defect phenotypes in zebrafish

We showed that disruption of centriolar satellite function in cultured cells affects the localization of cilium and centrosome proteins. To test whether centriolar satellites are important for cilium formation and function in vivo, we determined the effects of loss of centriolar satellites on zebrafish development. In zebrafish, disruption of cilium function results in phenotypes analogous to the clinical features of ciliopathies in humans, including pronephric cysts, retinal degeneration, Kupffer's vesicle abnormalities, and disrupted left–right asymmetry (Pazour *et al.*, 2000; Tsujikawa and Malicki, 2004; Sullivan-Brown *et al.*, 2008; Wilkinson *et al.*, 2009; Becker-Heck *et al.*, 2011). We determined the localization of zebrafish PCM1, using an antibody raised against the C-terminus of human PCM1 (Dammermann and Merdes, 2002). The human (Gene ID: 5108) and zebrafish (Gene ID: 321709) PCM1 amino acid sequences are 50% identical and 65% similar. In zebrafish PAC2/PC2 cells, PCM1 localized to small puncta distributed around the centrosome, similar to centriolar satellites in mammalian cells (Figure 6A), indicating functional conservation.

PCM1 was depleted from zebrafish embryos by injection of a morpholino antisense oligonucleotide directed against the start codon of the zebrafish PCM1 mRNA. At 48 h postfertilization (hpf), PCM1 morphant embryos displayed phenotypes characteristic of cilium dysfunction, including ventral and lateral body axis curvature, hydrocephaly (Figure 6B), and ectopic otoliths in the otic vesicles (Figure 6, B and C). Body axis curvature was highly penetrant, whereas ectopic otoltiths were observed in 40% of embryos and hydrocephaly in 30% ($n = 27$). Later during development, at 72 hpf, pronephric cysts were also apparent in some embryos (Figure 6D). To demonstrate specificity of the PCM1 morpholino, we tested whether human PCM1 could rescue the zebrafish embryo morphants. Zebrafish embryos were injected first in the yolk with the PCM1 translation-blocking morpholino, and then a portion of these embryos were injected in the cell with a plasmid construct encoding human PCM1 under the control of the cytomegalovirus (CMV) promoter. Embryos injected with morpholino alone displayed the expected phenotype, the most obvious aspect of which is a curved back (70%). Embryos that were also injected with the PCM1 construct resembled uninjected or water-injected control embryos with back curvature reduced (30%; $n = 27$ in each case). The phenotype generated by the PCM1 morpholino is therefore due to the specific depletion of this protein (Figure 6E).

Because PCM1 morphants had phenotypes characteristic of ciliary defects, we examined cilia organization and PCM1 localization in the pronephros. Morphant and control embryos were examined by whole-mount confocal immunofluorescence microscopy. PCM1 localized to centriolar satellites at the apical surface of ciliated cells (Figure 6F). In morphant embryos, PCM1 staining was absent, and cilia were reduced in length (Figure 6F). Morphants injected with a lower dose of morpholino (0.4 vs. 0.8 pmol of morpholino) had a milder phenotype, with shorter cilia present in patches next to areas of longer cilia. The length of cilia was correlated with degree of PCM1 depletion. At 24 hpf, cilia in control embryos had a length of 9.9 ± 1.3 μm ($n = 20$) (Figure 6, G and I), whereas cilia in PCM1 morphants were reduced in length by 65% (3.5 ± 1.5 μm, $n = 76$). We examined the cilia in Kupffer's vesicle at the 14-somite stage (Figure 6H). Cilia within Kupffer's vesicle in morphant embryos were less than half as long (1.8 ± 1.0 μm, $n = 20$) as in controls (4.1 ± 1.1 μm, $n = 20$; Figure 1, H and I). Inverted heart looping was observed in 46% ($n = 28$) of morphant embryos at 48 hpf, consistent with randomization of left–right asymmetry due to Kupffer's vesicle defects (unpublished data).

DISCUSSION

Centriolar satellites are conserved components of the vertebrate centrosome/cilium complex, but their function is poorly understood. Several ciliopathy-associated proteins localize to centriolar satellites (Lopes *et al.*, 2011), but the functional significance of this localization has not been tested. In this study, we sought to determine the cellular and developmental consequences of disrupting centriolar satellites and to address the molecular mechanism of their function. We identified Cep72 as a new component of centriolar satellites that is required for the recruitment of the ciliopathy-associated protein Cep290 to satellites. During ciliogenesis, the BBSome-associated protein BBS4 relocalizes from centriolar satellites to primary cilia (Kim *et al.*, 2004, 2008; Nachury *et al.*, 2007). Our results suggest that centriolar satellites negatively regulate ciliary recruitment of BBS4 and that Cep290 and Cep72 are critical for relocalization of

PCM1 RNAi expression constructs, fixed, and immunostained for ^{LAP}Cep72 (anti-GFP) and PCM1. The extent of ^{LAP}Cep72 relocalization to the pericentriolar material in PCM1 RNAi cells correlates with partial (middle) or complete (bottom) depletion of PCM1. DNA was stained with DAPI. Scale bars, 5 μm. (F) Immunolocalization of endogenous Cep72 and γ-tubulin in control (top) and PCM1-depleted HeLa cells (bottom). Scale bars, 1 μm. (G) Immunolocalization of endogenous Cep290 and γ-tubulin in control (top) and PCM1-depleted U2OS cells (bottom). Scale bars, 1 μm.

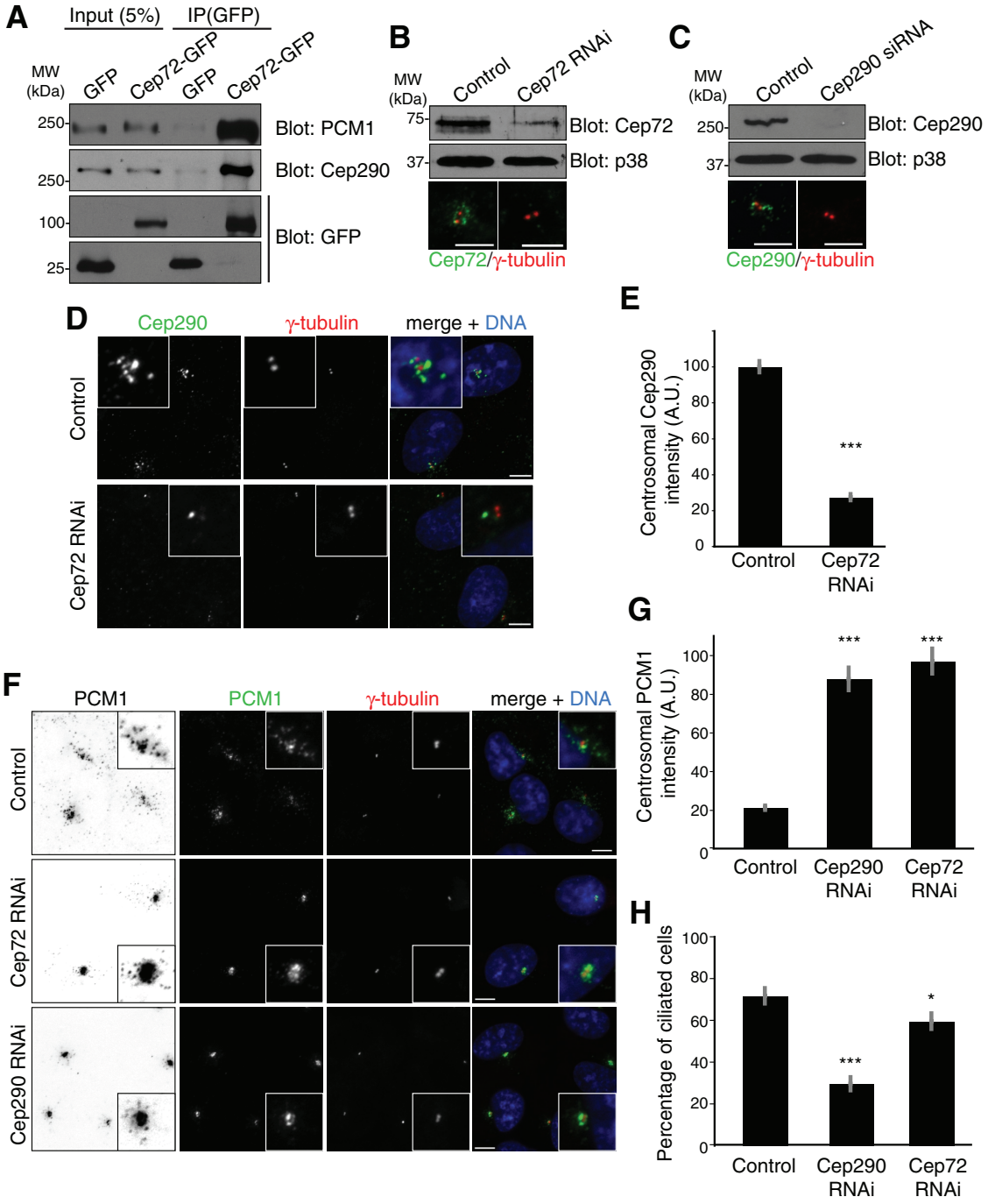

FIGURE 3: Cep72 is required for centriolar satellite localization of Cep290 and distribution of centriolar satellites. (A) GFP and CEP72-GFP were immunoprecipitated from extracts of HeLa cells transfected with each construct and analyzed by Western blot. Blots were probed for GFP and Cep72-GFP (anti-GFP), or endogenous PCM1 and Cep290. (B) HeLa cells were transfected with control siRNA or Cep72-targeting siRNA for 48 h. Cells were then fixed or used for preparation of extracts. Control or Cep72-depleted cell extracts were analyzed by Western blot and probed for Cep72 or p38 as a loading control. Fixed cells were immunostained for endogenous Cep72 and γ-tubulin. Scale bars, 3 μm. (C) Cells were transfected with control siRNA or siRNAs targeting Cep290 for 48 h. Depletion of Cep290 was verified by Western blot analysis of extracts from control or Cep290 RNAi cells, probing for Cep290, or p38 as a loading control. Fixed cells were immunostained for endogenous Cep290 and γ-tubulin. Scale bars, 3 μm. (D) Cep72 depletion reduces pericentrosomal localization of Cep290. hTERT-RPE1 cells were transfected with control or Cep72 siRNA for 48 h, fixed, and immunostained for endogenous Cep290 and γ-tubulin. DNA was stained with DAPI. Scale bars, 5 μm. (E) Cep290 fluorescence intensities were measured for control and Cep72-depleted cells in a 3.5-μm^2 circular area around the centrosome; levels are normalized to 100. $n = 105$ cells per group. Error bars, SEM. ***$p < 0.001$. (F) Depletion of Cep72 or Cep290 increases pericentrosomal recruitment of PCM1. hTERT-RPE1 cells were transfected with control, Cep72, or Cep290 siRNA for 48 h, fixed, and immunostained for endogenous PCM1 and γ-tubulin. DNA was stained with DAPI. Scale bars, 5 μm. (G) PCM1 fluorescence intensities were measured for control, Cep72-depleted, and Cep290-depleted

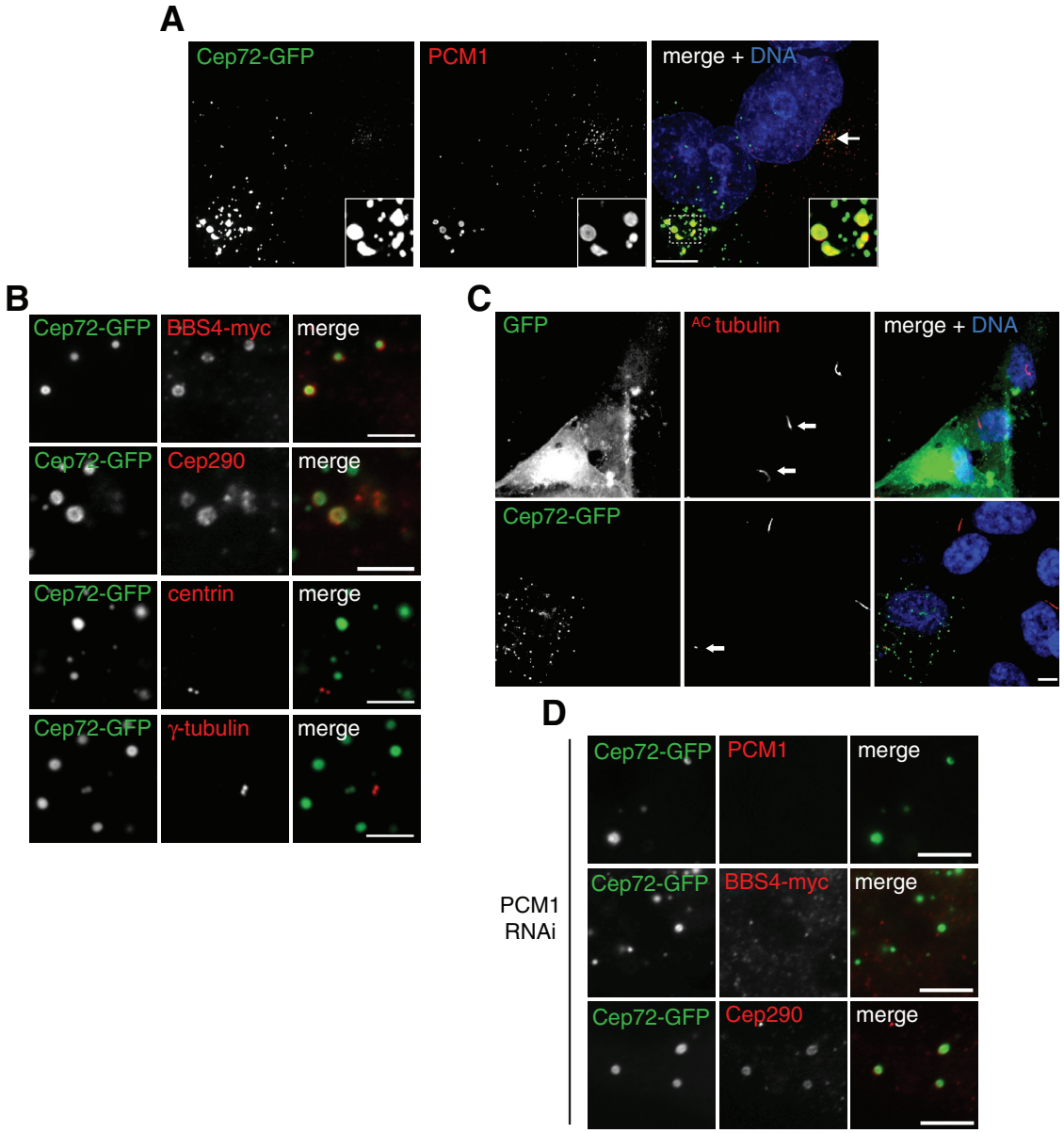

FIGURE 4: Overexpression of Cep72 mislocalizes centriolar satellite–associated proteins and interferes with cilium formation. (A) hTERT-RPE1 cells were transfected with Cep72-GFP, fixed, and immunostained for Cep72-GFP (anti-GFP) and endogenous PCM1. DNA was stained with DAPI. Scale bars, 5 μm. Cells had expression levels that ranged from low (right cell), in which Cep72-GFP colocalized with PCM1 in centriolar satellites, to high (left cell), in which Cep72-GFP formed large cytoplasmic aggregates that sequestered PCM1 (see inset). Images represent a deconvolved maximum projection of sections. (B) Cells were transfected with Cep72-GFP, fixed, and immunostained for BBS4-myc (anti-myc, in cells cotransfected with a construct expressing BBS4-myc; top), endogenous Cep290 (second from top), endogenous centrin (second from bottom), and endogenous γ-tubulin (bottom). Scale bars, 5 μm. (C) Ciliation was induced in GFP or Cep72-GFP–transfected hTERT-RPE1 cells transfected by serum starvation for 24 h. Cells were fixed and immunostained for Cep72-GFP (anti-GFP) or acetylated tubulin to mark centrioles and primary cilia. Percentage of ciliated cells in each case was determined over three experiments. Arrows indicate cilia/centrioles in transfected cells. (D) Cep290 is recruited to Cep72-GFP aggregates independent of PCM1. Cells were infected with control lentivirus or lentivirus expressing PCM1 shRNA and selected for infection. Cells were then transfected with Cep72-GFP, fixed, and immunostained for endogenous PCM1 (top), BBS4 (anti-myc, in cells cotransfected with a construct expressing BBS4-myc; middle), or endogenous Cep290 (bottom). Scale bars, 5 μm.

cells in a 3.5-μm^2 circular area around the centrosome; levels are normalized to 100. $n = 100$ cells per group. Error bars, SEM, ***$p < 0.001$. (H) Control, Cep290-depleted, and Cep72-depleted hTERT-RPE1 cells were serum starved for 24 h, fixed, and immunostained with an antibody against acetylated tubulin to label primary cilia. Percentage of ciliated cells was determined in each case. Control, $n = 700$; Cep290-depleted cells, $n = 400$; Cep72-depleted cells, $n = 500$. Error bars, SEM. ***$p < 0.001$, *$p < 0.05$.

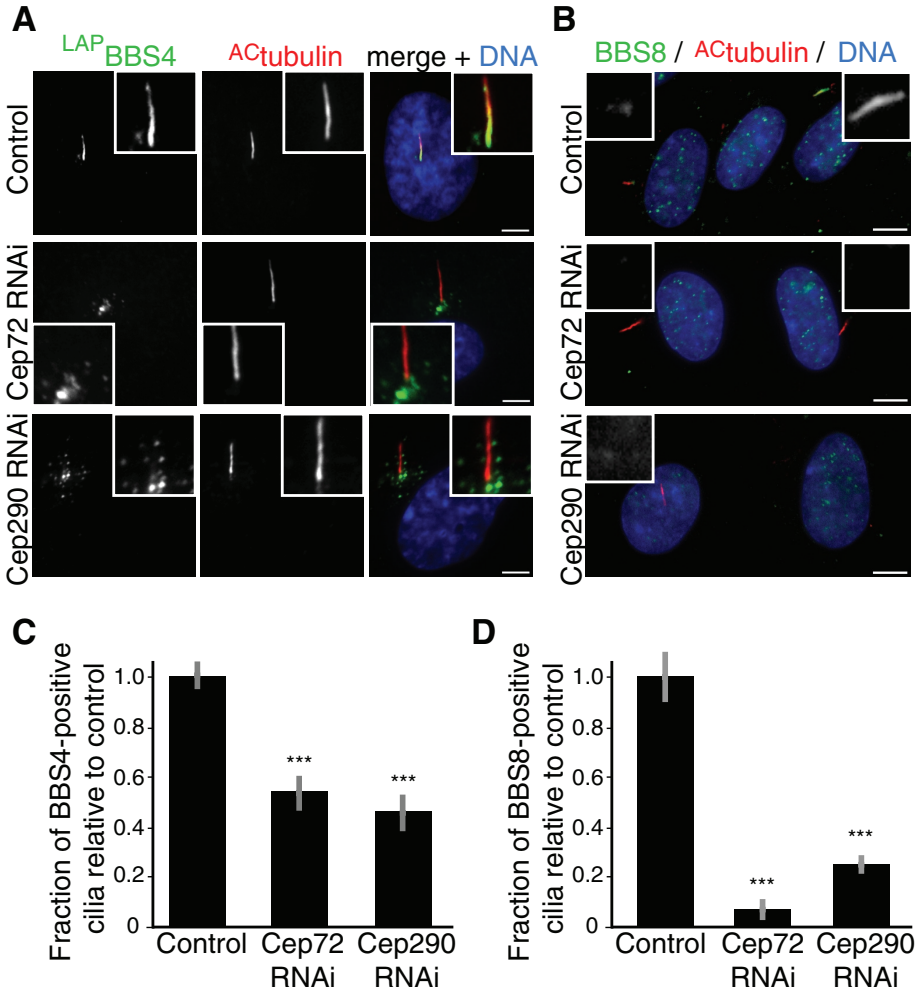

FIGURE 5: Depletion of Cep72 and Cep290 inhibits relocalization of BBS4 from centriolar satellites to primary cilia. (A) Depletion of Cep290 or Cep72 reduces efficiency of ^{LAP}BBS4 relocalization from centriolar satellites to primary cilia. ^{LAP}BBS4-hTERT-RPE1 cells were transfected with control, Cep72, or Cep290 siRNAs for 48 h, followed by overnight serum starvation. Cells were fixed and immunostained for ^{LAP}BBS4 (anti-GFP), and acetylated tubulin (^{AC}tubulin) to mark primary cilia. DNA was stained with DAPI. Scale bars, 5 μm. (B) Depletion of Cep290 or Cep72 impairs ciliary recruitment of BBS8. hTERT-RPE1 cells were transfected with control, Cep72, or Cep290 siRNAs for 48 h, followed by overnight serum starvation. Cells were fixed and immunostained for BBS8 (anti-BBS8) and acetylated tubulin to mark primary cilia. DNA was stained with DAPI. Cilia with BBS8 localized to the base of or throughout the length of the cilium were scored as positive. Ciliary BBS8 signal is shown in insets. Scale bars, 5 μm. (C, D) Fraction of ^{LAP}BBS4-positive (C) or BBS8-positive (D) cilia was determined for control, Cep72-depleted, and Cep290-depleted cells. Ciliary BBS8 signal is shown in insets (C). For ^{LAP}BBS4 results, $n = 300$ ciliated cells over three separate experiments. For BBS8 results, $n = 150$ over three separate experiments. Error bars, SEM. $p < 0.005$.

BBS4 from centriolar satellites to the cilium. We show that PCM1, the canonical component of mammalian centriolar satellites, also localizes to centriolar satellites in zebrafish cells and that depletion of zebrafish PCM1 leads to developmental defects in morphant embryos consistent with impaired cilium function (Kramer-Zucker *et al.*, 2005; Sayer *et al.*, 2006; Yen *et al.*, 2006; Leitch *et al.*, 2008). These results highlight the importance of centriolar satellites in regulation of cilium function and provide a new model for understanding how this regulation might be achieved.

We identified Cep72 as a PCM1-interacting protein that localizes to centriolar satellites. Cep72 and PCM1 have a similar pattern of evolutionary conservation, with orthologues present in hemichordates and placozoans but absent in arthropods, nematodes, and *Chlamydomonas*. PCM1 has been proposed to function as a scaffold for centriolar satellite recruitment of ciliopathy-associated proteins and in directing microtubule-dependent centrosome localization for some of these proteins (Kubo *et al.*, 1999; Kubo and Tsukita, 2003; Ge *et al.*, 2010). That the human PCM1 protein could largely rescue the zebrafish PCM1 morphant phenotype indicates conservation of PCM1 function in vertebrates. Mammals and some vertebrates have two Cep72-related paralogues: Cep72 and Lrrc36. In organisms with a single *CEP72/LRRC36* gene, the predicted protein is more similar to vertebrate Cep72, suggesting that it is the more ancestral sequence. An exception is that *Xenopus tropicalis* appears to have lost the Cep72 locus and maintained the Lrrc36 locus. This suggests the possibility that Lrrc36 might be able to substitute for Cep72's centriolar satellite function in *Xenopus*.

In contrast to the existing model implicating PCM1 in dynein-mediated localization of proteins to the centrosome, we found that loss of centriolar satellites by depletion of PCM1 stimulated centrosomal localization of two proteins, Cep72 and Cep290. In addition, we found that PCM1 was dispensable for ciliary recruitment of BBS4, ruling out the possibility that BBS4 is "delivered" to the centrosome via its association with PCM1 (Figure 7). These data suggest that for some proteins centriolar satellites can negatively regulate association with the centrosome.

Jin *et al.* (2010) proposed that PCM1 might negatively regulate the BBSome, restricting its ability to associate with membranes. This is based on the observation that PCM1 copurifies with BBS4 (Nachury *et al.*, 2007) but does not copurify with membrane-associated BBSome (Jin *et al.*, 2010). Our results suggest another possibility for regulation of the BBSome by centriolar satellites. Because BBS4 is the only BBSome component known to localize to satellites and is the final subunit added during BBSome assembly (Zhang *et al.*, 2012), sequestration of BBS4 by interaction with PCM1 at satellites might limit the amount of BBS4 available for incorporation into ciliary BBSomes. Thus the final assembly step for the BBSome and its subsequent ciliary localization and membrane association would require release of BBS4 from centriolar satellites (Figure 7). Consistent with this model, we demonstrate that ciliary recruitment of BBS4 still occurs in the absence of centriolar satellites (PCM1 depletion) and that it is compromised when Cep290 or Cep72 is depleted. Moreover, we find that ciliary recruitment of BBS8 is similarly compromised in Cep290- and Cep72-depleted cells, suggesting that BBSome recruitment itself may be defective. Thus we propose that assembly of BBS4 into the BBSome and subsequent ciliary

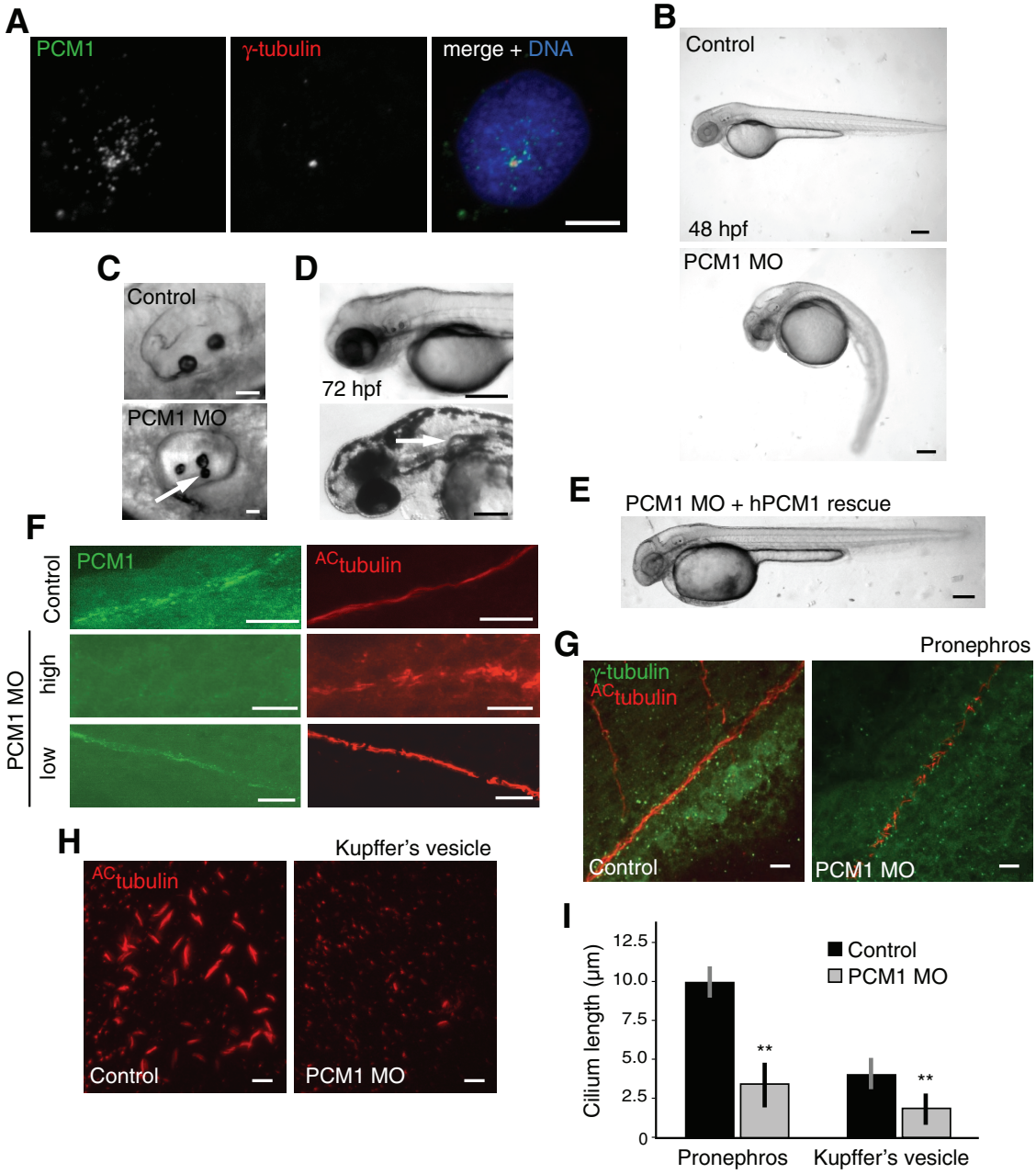

FIGURE 6: Loss of centriolar satellites affects cilium formation and causes developmental defects in zebrafish. (A) PCM1 localizes to centriolar satellites in zebrafish. PC2 cells were fixed and immunostained for PCM1 and γ-tubulin. DNA was stained with DAPI. Scale bars, 5 μm. (B) At 48 h postfertilization, PCM1 morphant embryos displayed ventral and lateral curvature of the body axis, hydrocephalus, and ectopic otoliths as compared with control embryos. (C) Lateral view of control and PCM1 morphant otic vesicles. Note extra otolith in the PCM1 morphant (arrow). (D) Control and PCM1 morphant pronephros at 72 hpf. Note cyst in the PCM1 morphant (arrow). (E) Coinjection of 100 ng/μl human ^{LAP}PCM1 expression construct and 0.8 pmol of PCM1 morpholino largely suppressed the PCM1 morphant phenotype. (F) Whole-mount immunofluorescence of PCM1 and pronephros cilia marked by acetylated tubulin (^{AC}tubulin) in control, high-dose PCM1 morphants (0.8 pmol; middle) and low-dose PCM1 morphants (0.4 pmol; bottom). In high-dose PCM1 morphants, PCM1 protein is completely depleted and cilia are reduced in length. Low-dose PCM1 morphants exhibit partial depletion and a milder cilia phenotype. (G, H) PCM1 morphant embryos have shorter cilia in the pronephros and Kupffer's vesicle as compared with control embryos. Whole-mount immunofluorescence staining of cilia in the pronephros (G) and Kupffer's vesicle (H) in control and PCM1 morphants (red, acetylated tubulin; green, γ-tubulin). (I) Quantitation of pronephros and Kupffer's vesicle cilia length in control and PCM1 morphant embryos. Scale bars, 100 μm (B, D, E), 10 μm (F–H).

recruitment of the BBSome is regulated by a mechanism involving Cep72 and Cep290 that occurs at the level of BBS4 relocalization from centriolar satellites (Figure 7).

BBS4 is believed to function as an adaptor that connects the dyenin–dynactin motor complex to PCM1 through an interaction with p150^{glued}. We found that depletion of either Cep72 or Cep290

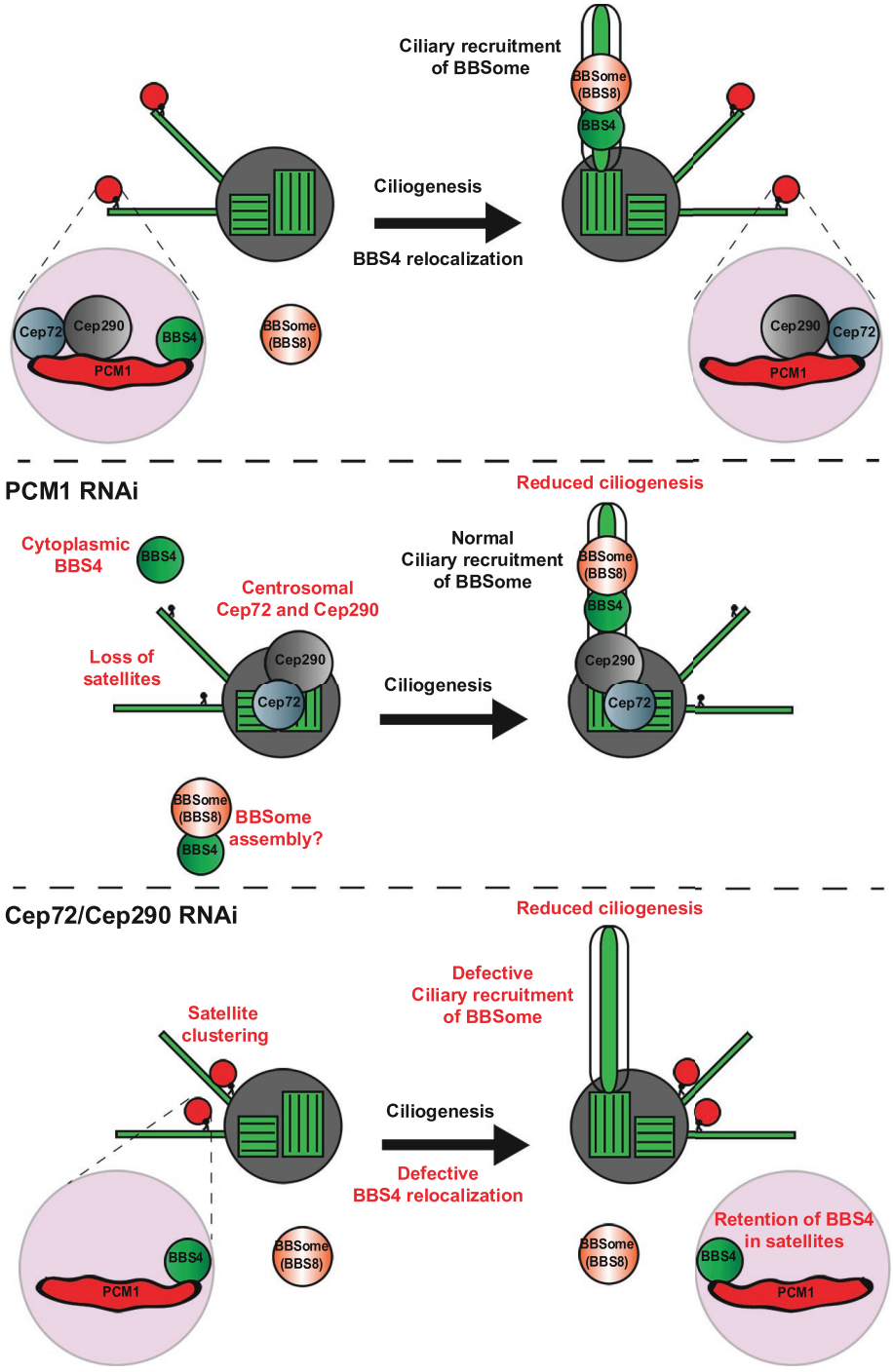

FIGURE 7: Summary and model. Regulation of BBSome localization by centriolar satellites. In a nonciliated cell (top, left), PCM1, Cep72, Cep290, and BBS4 localize to centriolar satellites. In ciliated cells (top, right), BBS4 relocalizes from centriolar satellites to the primary cilium and effects ciliary recruitment of other BBSome proteins (BBS8), whereas Cep290 and Cep72 are retained in centriolar satellites. In nonciliated PCM1-depleted cells (middle, left), centriolar satellites are lost, resulting in abnormal association of Cep72 and Cep290 with the centrosome. In ciliated PCM1-depleted cells, ciliary recruitment of the BBSome occurs normally. In nonciliated cells depleted of Cep72 or Cep290 (bottom, left), centriolar satellites retain BBS4 and accumulate irregularly around the centrosome. In ciliated cells depleted of Cep72 or Cep290 (bottom, right), release of BBS4 from centriolar satellites is defective, preventing ciliary localization of BBS4 and resulting in defective recruitment of other BBSome proteins (BBS8).

results in accumulation of PCM1 around centrosomes. In the case of Cep290, it had previously been proposed that this phenotype might result from an inability of PCM1 to interact with kinesin motors or an enhanced affinity of PCM1 for dynein motors (Kim *et al.*, 2008). The latter model is consistent with the observation that release of BBS4 from centriolar satellites is inefficient in cells depleted of Cep72 or Cep290. In addition, we found that disruption of satellites by overexpression of Cep72 resulted in cytoplasmic aggregates that sequestered BBS4 and Cep290. Sequestration of BBS4 but not Cep290 was dependent on PCM1. This suggests a possible hierarchy of assembly of centriolar satellite components.

How can we reconcile the proposed model, in which Cep290 functions as part of centriolar satellites with PCM1, with the broader evolutionary distribution of Cep290 relative to PCM1? One possibility is that centriolar satellites provide an additional mechanism for the regulation of the BBSome and other ciliary complexes and that the proposed "ciliary-gating" function of Cep290 at the transition zone (Craige *et al.*, 2010; Garcia-Gonzalo *et al.*, 2011) might also be occurring at centriolar satellites in organisms with PCM1. Alternatively, PCM1 could inhibit localization of Cep290 to the transition zone until ciliogenesis is initiated, temporally restricting its ciliary gating function.

Mutations in Cep290 have been identified in Bardet–Biedl syndrome and other ciliopathies. Our results suggest that such mutations might affect regulation of BBS4 and possibly other centriolar satellite–associated proteins. As an indication of the potential broader involvement of centriolar satellites in human disease, PCM1 has been reported to interact with other disease-associated proteins, including the schizophrenia-associated protein DISC1 (Kamiya *et al.*, 2008; Bradshaw and Porteous, 2010; Eastwood *et al.*, 2010), Huntingtin-interacting protein Hap1 (Engelender *et al.*, 1997), pericentrin, mutations in which contribute to primordial dwarfism and diabetes (Li *et al.*, 2001; Rauch *et al.*, 2008; Huang-Doran *et al.*, 2011), and as a fusion to the Jak2 kinase in leukemia (Bousquet *et al.*, 2005; Murati *et al.*, 2005). It will be interesting to determine whether these proteins are components of centriolar satellites and whether they work with PCM1, like Cep290 and Cep72, in the regulation of other proteins or are regulated by such an interaction.

MATERIALS AND METHODS

Antibodies, reagents, and transfections

Affinity-purified rabbit anti-human Cep72 antibody was purchased from Bethyl Laboratories (Montgomery, TX; A301-297A; peptide antigen, residues 150–200). Anti-Cep72 was diluted 1:500 for immunofluorescence and 1:2000 for Western blot. Rabbit anti-GFP antibody was generated

and used as previously described (Hatch *et al.*, 2010). Other antibodies used in this study were mouse anti–polyglutamylated tubulin (GT335; provided by C. Janke, Centre de Recherches de Biochemie Macromoléculaire, Montpellier, France), mouse anti–acetylated α-tubulin (6-11B-1; Abcam, Cambridge, MA) at 1:5000 for immunofluorescence, mouse anti-GFP (3e6; Invitrogen, Carlsbad, CA) at 1:500 for immunofluorescence, rat anti-GFP (Nacalai Tesque, Kyoto, Japan) at 1:2000 for immunofluorescence, mouse anti–centrin-2 (20H5; provided by J. Salisbury, Mayo Clinic, Rochester, MN) at 1:1000 for immunofluorescence, mouse anti-myc (9e10) at 1:500 for immunofluorescence, mouse anti–γ-tubulin (GTU-88; Sigma-Aldrich, St. Louis, MO) at 1:1000 for immunofluorescence, rabbit anti-BBS8 (SAB2103600; Sigma-Aldrich), rabbit anti-pericentrin at 1:500 for immunofluorescence as previously described (Luders *et al.*, 2006), rabbit anti-ninein (provided by M. Mogensen, University of East Anglia, Norwich, United Kingdom) at 1:500 for immunofluorescence, mouse anti–dynein IC (MAB1618; Millipore, Billerica, MA) at 1:500 for immunofluorescence, mouse anti–α-tubulin (DM1α; Sigma-Aldrich) at 1:500 for immunofluorescence and 1:1000 for Western blot, rabbit anti-PCM1 (provided by A. Merdes, Centre National de la Recherche Scientifique/Pierre Fabre, Toulouse, France) at 1:5000 for immunofluorescence and 1:10,000 for Western blot, rabbit anti-Cep290 (IHC-00365, Bethyl Laboratories) at 1:500 for immunofluorescence, rabbit anti-Cep290 (A301-659A, Bethyl Laboratories) at 1:2000 for Western blot, and rabbit anti-p38 (C-20; Santa Cruz Biotechnology, Santa Cruz, CA) at 1:2000 for Western blot. Purified rabbit immunoglobulin G (IgG) was purchased from Jackson ImmunoResearch Laboratories (West Grove, PA).

For microtubule-depolymerization experiments, cells were treated with 5 µg/ml nocodazole (US Biological, Swampscott, MA) or vehicle (dimethyl sulfoxide) for 3 h at 37°C. Plasmid transfections were performed using Lipofectamine 2000 according to the manufacturer's protocol (Invitrogen). For RNAi experiments, siRNAs were transfected with Lipofectamine RNAiMax according to the manufacturer's protocol (Invitrogen).

Plasmids, lentivirus, and RNAi

Full-length cDNAs for human Cep72 (GenBank accession no. NM_018140) and Lrrc36 (GenBank accession no. NM_018296) were obtained from ThermoFisher Scientific (Waltham, MA). Full-length cDNA for human PCM1 (GenBank accession no. NM_006197) was provided by R. Balczon (University of South Alabama, Mobile, AL). Full-length cDNA for human BBS4 (GenBank accession no. NM_033028) was provided by N. Katsanis (Duke University, Durham, NC). A pCMVβ-p50-dynamitin-myc plasmid was used for p50-dynamitin overexpression (Echeverri *et al.*, 1996). Open reading frames of Cep72, Lrrc36, PCM1, and BBS4 were PCR amplified, verified by sequencing, and cloned into pEGFP-N1 (Clontech, Mountain View, CA) or a pEGFP-N1–derived plasmid in which GFP is replaced with a Myc-hemagglutinin (HA)-histidine (His) tag. These plasmids were created in pTS1919 and pTS1920 (respectively Cep72-GFP and -mycHAHis), pTS1949 (Lrrc36GFP), pTS1681 (PCM1-mycHAHis), and pTS1686 (BBS4-mycHAHis). To generate the LAP (GFP-Tev-S-tag)-Cep72 and -PCM1 constructs, we cloned the Cep72 or PCM1 cDNA into pMN444 pEF5-FRT-LapC DEST, provided by M. Nachury (Stanford University, Stanford, CA), using Gateway technology (Invitrogen) to create pTS2047 and pTS2019, respectively. For bacterial expression of Cep72 GST-fusion protein, the Cep72 cDNA was cloned in pGex-4T-1 (GE Healthcare Biosciences, Piscataway, NJ) to create pTS1929. To generate Cep72 deletion constructs, Cep72 cDNA was PCR amplified and cloned into pEGFP-N1 (Clontech) according to sequences corresponding to amino acids 1–96 (pTS 2088), 1–135 (pTS2110), 136–647 (pTS2111), 489–647 (pTS2091), and 136–488 (pTS2120), followed by sequence verification.

PCM1 depletion was carried out using a 19-mer short hairpin RNA (shRNA) targeting the sequence of human PCM1, 5′-GTATCACATCTGAACTAAA-3′ (pTS2063), or mouse PCM1, 5′-GCATCACATCTGAACTAAA-3′, as described previously (Vladar and Stearns, 2007). PCM1 shRNA oligos were designed using pSicoOligomaker 1.5, annealed, and subcloned into the lentiviral vector pSicoR-puro (Ventura *et al.*, 2004), which confers puromycin resistance. PCM1 depletion was carried out by direct transfection of this plasmid or by infection of cells with shRNA-expressing lentivirus, generated as previously described (Mahjoub *et al.*, 2010), using this plasmid as a transfer vector. For plasmid or lentiviral controls, cells were transfected with pSicoR-puro vector or infected with lentivirus generated using pSicoR-puro as the transfer vector, respectively. Transfected cells were allowed to recover for 72 h posttransfection and analyzed for depletion. Lentivirus-infected cells were selected for 4 d in 3 µg/ml puromycin (Sigma-Aldrich), split, and maintained in selection for the duration of the experiment. Cep72 depletion was carried out using transfection of a previously described human Cep72 siRNA (Oshimori *et al.*, 2009), targeting the following sequence: 5′-TTGCAGATCGCTGGACTTCAA-3′ (Thermo Scientific, Waltham, MA). Cells were transfected as described for 48 h and then analyzed for depletion. Depletion of human Cep290 was carried out by transfection of ON-TARGET Plus SMARTpool (Thermo Scientific), as described previously (Kim *et al.*, 2008). Cells were transfected as described for 48 h and then analyzed for depletion. An siRNA targeting luciferase was used as control (Thermo Scientific).

Cell extracts, Western blotting, and immunoprecipitation

Whole-cell extracts for Western blotting were prepared by washing cells in phosphate-buffered saline (PBS), followed by lysis in SDS sample buffer. To prepare extracts for immunoprecipitation, cells were washed with cold PBS and lysed in LAP200 buffer (50 mM 4-(2-hydroxyethyl)-1-piperazineethanesulfonic acid, pH 7.4, 100 mM KCl, 1 mM ethylene glycol tetraacetic acid, 1 mM $MgCl_2$, 10% glycerol, and 0.3% NP40) containing a protease inhibitor cocktail (Roche, Indianapolis, IN) at 4°C for 20 min. Extracts were clarified by centrifugation, and 5% of extract was removed for input samples and lysed in SDS sample buffer. Remaining extract was transferred to polypropylene tubes and incubated with ~1 µg of relevant antibody, rotating for 3 h at 4°C. After incubation with antibody, 40 µl of 50% protein G–Sepharose (GE Healthcare) was added, and samples were rotated for 1 h at 4°C. Beads were then pelleted and resuspended three times in LAP200 buffer before pelleting and resuspension in SDS sample buffer. Inputs and bound proteins were resolved by SDS–PAGE and transferred to nitrocellulose membrane (Bio-Rad, Hercules, CA). Membranes were blocked with 5% milk, washed with Tris-buffered saline containing 0.5% Tween20 (Sigma-Aldrich) and probed with primary antibodies. Bound primary antibodies were detected using secondary antibodies conjugated to horseradish peroxidase (GE Healthcare), using chemiluminescence reagents (Thermo Scientific).

Cell lines, transfections, and drugs

HeLa, U2OS, 293, and NIH 3T3 cells were grown in DM (Invitrogen) supplemented with 10% fetal bovine serum (FBS; Atlanta Biologicals, Lawrenceville, GA). hTERT-RPE1 and IMCD3 cells were grown in DME/F12 (Invitrogen) supplemented with 10% FBS. All cells were cultured at 37°C and 5% CO_2. ^{LAP}BBS4-hTERT-RPE1 and GFP-Rab8-hTERT-RPE1 cells were provided by M. Nachury (Stanford University, Stanford, CA). Stably expressing ^{LAP}Cep72-IMCD3 cells were generated by cotransfecting IMCD3 Flp-in cells (Invitrogen) with

pOG44 (Invitrogen), followed by selection with 10 µg/ml hygromycin B (Invitrogen). Lrrc36-GFP-hTERT-RPE1 stable cell lines were generated by transfecting hTERT-RPE1 cells with pEGFP-N1 Lrrc36, followed by selection with 10 µg/ml Geneticin. For primary cilium formation experiments, cells were cultured under serum starvation conditions (0.5% FBS).

Immunofluorescence and microscopy

For immunofluorescence experiments, cells were grown on coverslips coated with poly-L-lysine, washed with PBS, and fixed in either 4% paraformaldehyde in PBS at room temperature or in –20°C methanol for 10 min. After fixation, cells were washed with PBS, followed by extraction and blocking with PBS containing 3% bovine serum albumin (Sigma-Aldrich), 0.1% Triton X-100, and 0.02% sodium azide (PBS-BT). Coverslips were incubated sequentially with primary antibodies diluted in PBS-BT for 1 h at room temperature or overnight at 4°C. Alexa Fluor dye–conjugated secondary antibodies (Invitrogen) were diluted in PBS-BT 1:250 and incubated sequentially at room temperature for 1 h. In cases in which cells were labeled with two mouse monoclonal antibodies, appropriate isotype-specific secondary antibodies were used to distinguish the antibodies (Invitrogen). Coverslips were mounted using antifade mounting media containing PBS, glycerol, and *p*-phenylenediamine. For standard immunofluorescence, images were acquired with Openlab 4.0.4 (PerkinElmer, Waltham, MA), using an Axiovert 200M microscope (Carl Zeiss, Jena, Germany). Images were processed using Photoshop (Adobe Systems, San Jose, CA).

For deconvolution microscopy, *z*-stacks of ~2-µm-thick sections with 0.5-µm intervals were captured using a 100×/1.35 numerical aperture objective with an IX70 microscope (Olympus, Tokyo, Japan) controlled by a DeltaVision imaging station (Applied Precision, Issaquah, WA) maintained by the Cell Sciences Imaging Facility (Stanford University, Stanford, CA). Images were deconvolved using the DeltaVision constrained iterative algorithm and point-spread functions. Three-dimensional volumes were used to generate movies, and maximum-intensity projections were assembled using the DeltaVision software.

Quantitation and statistical analysis

Quantitative immunofluorescence for PCM1 and Cep290 was performed on cells by acquiring single-plane images of control and depleted cells using identical gain and exposure settings, determined by adjusting settings based on the fluorescence signal in the control cells. Although centriolar satellites are distributed in three dimensions, these single-plane images captured most of the satellite fluorescence, due to the limited thickness of the cells. The region of interest in the images was defined as a circular 3.5-µm^2 area centered on the centrosome (indicated by γ-tubulin staining) in each cell. This region encompassed the majority of pericentrosomal satellites in these cells. Average pixel intensity of fluorescence within the region of interest was measured using ImageJ (National Institutes of Health, Bethesda, MD). Primary cilium formation was assessed by counting the total number of cells and the number of cells with primary cilia, as detected by acetylated or glutamylated tubulin staining. Statistical analysis was performed using Student's *t* tests in Excel (Microsoft, Redmond, WA). Error bars reflect SEM.

Zebrafish

For zebrafish cell culture, cells were grown in DME/F12 (Invitrogen) supplemented with 10% FBS and 1% penicillin/streptomycin at 30°C and 6% CO_2. TL wild-type zebrafish were maintained and bred at 27°C; embryos were raised at 28.5°C, as described by Westerfield (1993). Embryos were injected with morpholinos using a micromanipulator-mounted micropipette (Borosil 1.0 × 0.5 mm; Harvard Apparatus, Holliston, MA) and a World Precision Instruments (Sarasota, FL) microinjector. Between 1 and 5 nl of solution was injected into the yolk of embryos. Morpholinos directed against the zebrafish orthologue of PCM1 (Gene ID: 321709) were purchased from Gene Tools (Philomath, OR), MOPCM1st, 5′-TGGAGTGCCACCCGTTGCCATGATG-3′. Controls were performed with volume-matched injections of solvent.

For whole-mount immunostaining, embryos were permeabilized by incubation in 0.25% trypsin-EDTA in Hank's balanced salt solution (Life Technologies, Invitrogen) for 10 min on ice and then washed three times for 30 min in PBS plus 0.2% Triton to remove the enzyme. Embryos were blocked by incubation for 4 h in 10% heat-inactivated goat serum, 1% bovine serum albumin, and 0.2% Triton X-100 in PBS. Embryos were incubated with primary and secondary antibodies for 36 h in blocking solution. The primary antibodies were rabbit anti–γ-tubulin (5192, Sigma-Aldrich), 0.6 µg/ml, and mouse anti–acetylated-tubulin 6-11B-1 (Invitrogen), 1 µg/ml. Secondary antibodies used were goat anti-mouse IgG, Cy3-conjugated (Invitrogen), 1 µg/ml, and goat anti-rabbit IgG, Alexa 488-conjugated (Invitrogen), 2 µg/ml. Photomicrography was performed with a Nikon upright microscope (Nikon, Melville, NY), equipped with a GXCAM-3 charge-coupled device camera. Confocal stacks were imaged with an Olympus FX81/FV1000 laser confocal system using Ar gas laser and He–Ne diode laser. Stacks were analyzed using ImageJ. Stacks were taken in 1-µm sections and are represented as maximum-intensity projections.

ACKNOWLEDGMENTS

We thank Y. L. Lee for generating the rabbit anti-GFP antibody, the Stanford University Cell Sciences Imaging Facility and Jon Mulholland for assistance with deconvolution microscopy, M. Nachury for reagents and helpful advice, and G. Hughes for technical help with aquariums. A.I. was a Master's student on a joint Royal Holloway and St George's Master's Program. This work was supported by a Research Grant from the Royal Society and by the Royal Holloway Research Strategy Fund (to C.J.W.), the National Science Foundation Graduate Research Fellowship Program (T.R.S.), a Stanford Graduate Fellowship in the Cancer Biology Program (T.R.S.), and National Institutes of Health Grant GM52022 (to T.S).

REFERENCES

Andersen JS, Wilkinson CJ, Mayor T, Mortensen P, Nigg EA, Mann M (2003). Proteomic characterization of the human centrosome by protein correlation profiling. Nature 426, 570–574.

Baala L *et al.* (2007). Pleiotropic effects of CEP290 (NPHP6) mutations extend to Meckel syndrome. Am J Hum Genet 81, 170–179.

Badano JL, Mitsuma N, Beales PL, Katsanis N (2006). The ciliopathies: an emerging class of human genetic disorders. Annu Rev Genomics Hum Genet 7, 125–148.

Baker K, Beales PL (2009). Making sense of cilia in disease: the human ciliopathies. Am J Med Genet C Semin Med Genet 151C, 281–295.

Balczon R, Bao L, Zimmer WE (1994). PCM-1, A 228-kD centrosome autoantigen with a distinct cell cycle distribution. J Cell Biol 124, 783–793.

Becker-Heck A *et al.* (2011). The coiled-coil domain containing protein CCDC40 is essential for motile cilia function and left-right axis formation. Nat Genet 43, 79–84.

Bousquet M, Quelen C, De Mas V, Duchayne E, Roquefeuil B, Delsol G, Laurent G, Dastugue N, Brousset P (2005). The t(8;9)(p22;p24) translocation in atypical chronic myeloid leukaemia yields a new PCM1-JAK2 fusion gene. Oncogene 24, 7248–7252.

Bradshaw NJ, Porteous DJ (2010). DISC1-binding proteins in neural development, signalling and schizophrenia. Neuropharmacology 62, 1230–1241.

Brancati F *et al.* (2007). CEP290 mutations are frequently identified in the oculo-renal form of Joubert syndrome-related disorders. Am J Hum Genet 81, 104–113.

Chang B *et al.* (2006). In-frame deletion in a novel centrosomal/ciliary protein CEP290/NPHP6 perturbs its interaction with RPGR and results in early-onset retinal degeneration in the rd16 mouse. Hum Mol Genet 15, 1847–1857.
Coppieters F, Lefever S, Leroy BP, De Baere E (2010). CEP290, a gene with many faces: mutation overview and presentation of CEP290base. Hum Mutat 31, 1097–1108.
Craige B, Tsao CC, Diener DR, Hou Y, Lechtreck KF, Rosenbaum JL, Witman GB (2010). CEP290 tethers flagellar transition zone microtubules to the membrane and regulates flagellar protein content. J Cell Biol 190, 927–940.
Dammermann A, Merdes A (2002). Assembly of centrosomal proteins and microtubule organization depends on PCM-1. J Cell Biol 159, 255–266.
Eastwood SL, Walker M, Hyde TM, Kleinman JE, Harrison PJ (2010). The DISC1 Ser704Cys substitution affects centrosomal localization of its binding partner PCM1 in glia in human brain. Hum Mol Genet 19, 2487–2496.
Echeverri CJ, Paschal BM, Vaughan KT, Vallee RB (1996). Molecular characterization of the 50-kD subunit of dynactin reveals function for the complex in chromosome alignment and spindle organization during mitosis. J Cell Biol 132, 617–633.
Engelender S, Sharp AH, Colomer V, Tokito MK, Lanahan A, Worley P, Holzbaur EL, Ross CA (1997). Huntingtin-associated protein 1 (HAP1) interacts with the p150Glued subunit of dynactin. Hum Mol Genet 6, 2205–2212.
Garcia-Gonzalo FR *et al.* (2011). A transition zone complex regulates mammalian ciliogenesis and ciliary membrane composition. Nat Genet 43, 776–784.
Ge X, Frank CL, Calderon de Anda F, Tsai LH (2010). Hook3 interacts with PCM1 to regulate pericentriolar material assembly and the timing of neurogenesis. Neuron 65, 191–203.
Gerdes JM, Davis EE, Katsanis N (2009). The vertebrate primary cilium in development, homeostasis, and disease. Cell 137, 32–45.
Hatch EM, Kulukian A, Holland AJ, Cleveland DW, Stearns T (2010). Cep152 interacts with Plk4 and is required for centriole duplication. J Cell Biol 191, 721–729.
Hildebrandt F, Benzing T, Katsanis N (2011). Ciliopathies. N Engl J Med 364, 1533–1543.
Hodges ME, Scheumann N, Wickstead B, Langdale JA, Gull K (2010). Reconstructing the evolutionary history of the centriole from protein components. J Cell Sci 123, 1407–1413.
Huang-Doran I *et al.* (2011). Genetic defects in human pericentrin are associated with severe insulin resistance and diabetes. Diabetes 60, 925–935.
Huangfu D, Liu A, Rakeman AS, Murcia NS, Niswander L, Anderson KV (2003). Hedgehog signalling in the mouse requires intraflagellar transport proteins. Nature 426, 83–87.
Hunkapiller J, Singla V, Seol A, Reiter JF (2010). The ciliogenic protein Ofd1 regulates the neuronal differentiation of embryonic stem cells. Stem Cells Dev 20, 831–841.
Jin H, White SR, Shida T, Schulz S, Aguiar M, Gygi SP, Bazan JF, Nachury MV (2010). The conserved Bardet-Biedl syndrome proteins assemble a coat that traffics membrane proteins to cilia. Cell 141, 1208–1219.
Kamiya A *et al.* (2008). Recruitment of PCM1 to the centrosome by the cooperative action of DISC1 and BBS4: a candidate for psychiatric illnesses. Arch Gen Psychiatry 65, 996–1006.
Kim J, Krishnaswami SR, Gleeson JG (2008). CEP290 interacts with the centriolar satellite component PCM-1 and is required for Rab8 localization to the primary cilium. Hum Mol Genet 17, 3796–3805.
Kim JC *et al.* (2004). The Bardet-Biedl protein BBS4 targets cargo to the pericentriolar region and is required for microtubule anchoring and cell cycle progression. Nat Genet 36, 462–470.
Kodani A, Tonthat V, Wu B, Sutterlin C (2010). Par6 alpha interacts with the dynactin subunit p150 Glued and is a critical regulator of centrosomal protein recruitment. Mol Biol Cell 21, 3376–3385.
Kramer-Zucker AG, Olale F, Haycraft CJ, Yoder BK, Schier AF, Drummond IA (2005). Cilia-driven fluid flow in the zebrafish pronephros, brain and Kupffer's vesicle is required for normal organogenesis. Development 132, 1907–1921.
Kubo A, Tsukita S (2003). Non-membranous granular organelle consisting of PCM-1: subcellular distribution and cell-cycle-dependent assembly/disassembly. J Cell Sci 116, 919–928.
Kubo A, Sasaki H, Yuba-Kubo A, Tsukita S, Shiina N (1999). Centriolar satellites: molecular characterization, ATP-dependent movement toward centrioles and possible involvement in ciliogenesis. J Cell Biol 147, 969–980.
Lechtreck KF, Johnson EC, Sakai T, Cochran D, Ballif BA, Rush J, Pazour GJ, Ikebe M, Witman GB (2009). The *Chlamydomonas reinhardtii* BBSome is an IFT cargo required for export of specific signaling proteins from flagella. J Cell Biol 187, 1117–1132.
Leitch CC *et al.* (2008). Hypomorphic mutations in syndromic encephalocele genes are associated with Bardet-Biedl syndrome. Nat Genet 40, 443–448.
Li Q, Hansen D, Killilea A, Joshi HC, Palazzo RE, Balczon R (2001). Kendrin/pericentrin-B, a centrosome protein with homology to pericentrin that complexes with PCM-1. J Cell Sci 114, 797–809.
Lopes CA, Prosser SL, Romio L, Hirst RA, O'Callaghan C, Woolf AS, Fry AM (2011). Centriolar satellites are assembly points for proteins implicated in human ciliopathies, including oral-facial-digital syndrome 1. J Cell Sci 124, 600–612.
Luders J, Patel UK, Stearns T (2006). GCP-WD is a gamma-tubulin targeting factor required for centrosomal and chromatin-mediated microtubule nucleation. Nat Cell Biol 8, 137–147.
Mahjoub MR, Xie Z, Stearns T (2010). Cep120 is asymmetrically localized to the daughter centriole and is essential for centriole assembly. J Cell Biol 191, 331–346.
Murati A *et al.* (2005). PCM1-JAK2 fusion in myeloproliferative disorders and acute erythroid leukemia with t(8;9) translocation. Leukemia 19, 1692–1696.
Mykytyn K, Mullins RF, Andrews M, Chiang AP, Swiderski RE, Yang B, Braun T, Casavant T, Stone EM, Sheffield VC (2004). Bardet-Biedl syndrome type 4 (BBS4)-null mice implicate Bbs4 in flagella formation but not global cilia assembly. Proc Natl Acad Sci USA 101, 8664–8669.
Nachury MV *et al.* (2007). A core complex of BBS proteins cooperates with the GTPase Rab8 to promote ciliary membrane biogenesis. Cell 129, 1201–1213.
Oshimori N, Li X, Ohsugi M, Yamamoto T (2009). Cep72 regulates the localization of key centrosomal proteins and proper bipolar spindle formation. EMBO J 28, 2066–2076.
Pazour GJ, Baker SA, Deane JA, Cole DG, Dickert BL, Rosenbaum JL, Witman GB, Besharse JC (2002). The intraflagellar transport protein, IFT88, is essential for vertebrate photoreceptor assembly and maintenance. J Cell Biol 157, 103–113.
Pazour GJ, Dickert BL, Vucica Y, Seeley ES, Rosenbaum JL, Witman GB, Cole DG (2000). *Chlamydomonas* IFT88 and its mouse homologue, polycystic kidney disease gene tg737, are required for assembly of cilia and flagella. J Cell Biol 151, 709–718.
Pedersen LB, Rosenbaum JL (2008). Intraflagellar transport (IFT) role in ciliary assembly, resorption and signalling. Curr Top Dev Biol 85, 23–61.
Rauch A *et al.* (2008). Mutations in the pericentrin (PCNT) gene cause primordial dwarfism. Science 319, 816–819.
Rual JF *et al.* (2005). Towards a proteome-scale map of the human protein-protein interaction network. Nature 437, 1173–1178.
Sayer JA *et al.* (2006). The centrosomal protein nephrocystin-6 is mutated in Joubert syndrome and activates transcription factor ATF4. Nat Genet 38, 674–681.
Schneider L, Clement CA, Teilmann SC, Pazour GJ, Hoffmann EK, Satir P, Christensen ST (2005). PDGFRalphaalpha signaling is regulated through the primary cilium in fibroblasts. Curr Biol 15, 1861–1866.
Sullivan-Brown J, Schottenfeld J, Okabe N, Hostetter CL, Serluca FC, Thiberge SY, Burdine RD (2008). Zebrafish mutations affecting cilia motility share similar cystic phenotypes and suggest a mechanism of cyst formation that differs from pkd2 morphants. Dev Biol 314, 261–275.
Tsang WY, Bossard C, Khanna H, Peranen J, Swaroop A, Malhotra V, Dynlacht BD (2008). CP110 suppresses primary cilia formation through its interaction with CEP290, a protein deficient in human ciliary disease. Dev Cell 15, 187–197.
Tsujikawa M, Malicki J (2004). Intraflagellar transport genes are essential for differentiation and survival of vertebrate sensory neurons. Neuron 42, 703–716.
Valente EM *et al.* (2006). Mutations in CEP290, which encodes a centrosomal protein, cause pleiotropic forms of Joubert syndrome. Nat Genet 38, 623–625.
Ventura A, Meissner A, Dillon CP, McManus M, Sharp PA, Van Parijs L, Jaenisch R, Jacks T (2004). Cre-lox-regulated conditional RNA interference from transgenes. Proc Natl Acad Sci USA 101, 10380–10385.
Vladar EK, Stearns T (2007). Molecular characterization of centriole assembly in ciliated epithelial cells. J Cell Biol 178, 31–42.
Westerfield M (1993). The Zebrafish Book: A Guide for the Laboratory Use of Zebrafish (*Brachydanio rerio*), Eugene, OR: M. Westerfield.
Wilkinson CJ, Carl M, Harris WA (2009). Cep70 and Cep131 contribute to ciliogenesis in zebrafish embryos. BMC Cell Biol 10, 17.
Yen HJ, Tayeh MK, Mullins RF, Stone EM, Sheffield VC, Slusarski DC (2006). Bardet-Biedl syndrome genes are important in retrograde intracellular trafficking and Kupffer's vesicle cilia function. Hum Mol Genet 15, 667–677.
Zhang Q, Yu D, Seo S, Stone EM, Sheffield VC (2012). Intrinsic protein-protein interaction-mediated and chaperonin-assisted sequential assembly of a stable Bardet Biedl syndrome protein complex, the BBSome. J Biol Chem 287, 20625–20635.